

PROPELLER INSTALLATION EFFECTS ON MULTI-ENGINE PROPELLER AIRCRAFT DIRECTIONAL STABILITY AND CONTROL

M.J.T. Schroyen , R. Slingerland

Department of Design, Integration and Operations of Aircraft and Rotorcraft

Faculty of Aerospace Engineering

Delft University of Technology

P.O. Box 5058 2600 GB

Delft, The Netherlands

Phone: +31 152785332

M.J.T.Schroyen@student.tudelft.nl,

R.Slingerland@lr.tudelft.nl

Keywords: *Propeller, Slipstream, directional stability (no more than 5)*

Abstract

Propulsive efficiency is becoming important in aircraft design due to depletion of the oil reserves. Propeller propulsion is beneficial in this respect, but has a negative influence on the stability and control of multi-engine aircraft.

The objectives of this paper are limited to the propeller installation effects on the directional stability and control characteristics in the preliminary design phase based on classical aerodynamic theory.

The aircraft components, the propeller, nacelles, wing, flaps, fuselage and tail and their effect on each other are modelled by potential theory. Potential theory is used because it is linear and allows for a modular calculation scheme. Comparing the calculated and measured yawing moment shows an adequately modelled configuration without flaps. For the configuration with flaps deployed the model gives an underestimation in yawing moment coefficient of about 30%. The differences are contributed to an incorrectly calculated wing lift distribution with

one live engine. The consequence is an incorrect wing trailing vortex sheet shape and strength. Further study also revealed that the wing trailing vortex sheet model is invalid in regions of large induced velocities, in particular at the inboard tip of the flap. These three effects result in an incorrect cross flow at the vertical tail, which causes an underestimation of the tail loading.

Nomenclature

\hat{A}	Influence matrix [—]
a, a'	Velocity increments due to the propeller [—]
c_{d_0}	Profile drag coefficient [—]
c_{l_α}	Lift curve slope [1/rad]
c_n	Yawing moment coefficient $\frac{N}{\frac{1}{2}\rho V^2 S b}$ [—]
c_x, c_y	Force coefficient [—]
c	Chord length [m]
C	Prandtl correction factor [—]
D	Drag [N]
E	Fraction of the flap to the total chord [—]
F	Fuselage [—]
F_y	Side force [N]
i, j	Panel index [—]
(L, M, N)	Moments [Nm]
N_b	Number of propeller blades [—]

\vec{n}	Unit vector normal to the surface [–]
p_t	Total pressure [N/m^2]
Q	Propeller torque [Nm]
R	Outer radius [m]
r	Radius [m]
S_{14}, S_{23}	Panel side slope [–]
S	Surface area [m^2]
T	Thrust [N]
T_c	Thrust coefficient, Equation 10 [–]
u	General variable [–]
V	Total velocity [m/s]
\vec{v}	Additional velocity [m/s]
w	Panel width [m]
(x, y, z)	Coordinates [m]
α, β	Angle of attack, side slip angle [rad]
Γ	Vortex strength [m^2/s]
γ	Vorticity density [m/s]
δ	Flap deflection angle [rad]
λ	Advance coefficient [–]
(ξ, η, ζ)	Panel reference frame [–]
ρ	Density [kg/m^3]
σ	Propeller solidity [–]
ϕ, θ	Propeller blade angle [rad]
Ω	Circumferential velocity [rad/s]

1 Introduction

Depletion of the oil reserves forces aircraft designers to investigate methods of increasing the efficiency of aircraft. For the propulsive efficiency it is beneficial to increase the velocity of a large amount of air by a small amount. In this respect propeller propulsion has an advantage over jet propulsion. Influencing a large amount of air however is disadvantageous because it changes the aerodynamics about the aircraft considerably. In particular the stability and control of multi-engine aircraft deteriorate due to these interference effects. The critical design condition is a high thrust setting with one engine inoperative. The objectives are to create a model to estimate the installation effects of multiple propellers on the aircraft's directional stability and control characteristics in the preliminary design phase. Therefore classical aerodynamic theory has been

called upon and has been implemented in a Matlab code.

This paper is structured as follows: the components of the model are discussed and compared to wind-tunnel measurements performed by Manée. First the propeller, nacelle and wing model are discussed. For the propeller/nacelle/wing model, with and without flaps, the calculation results are compared to measurement data. To model the configuration with tail, the flow field behind the wing and its effect on the vertical tail are studied. The calculation results of this configuration are also compared to measurement data. The fuselage is added to the model and the results are again compared to wind-tunnel measurement data. Finally conclusions are drawn.

2 Propeller model

The propeller model is based on vortex theory. This theory is a refinement of the blade element theory and includes the effects of the propeller slipstream onto the propeller disc. Also included, with an iteration loop, are the effects of the wing and fuselage on the propeller disc. Combining the resulting equations gives an implicit function for the blade element angle ϕ [9],

$$\frac{\cos \phi + \frac{\sigma}{4C \sin \phi} ((\theta - \phi) c_{l\alpha} \sin \phi + c_{d0} \cos \phi)}{\sin \phi - \frac{\sigma}{4C \sin \phi} ((\theta - \phi) c_{l\alpha} \cos \phi - c_{d0} \sin \phi)} = \frac{r \Omega}{V}, \quad (1)$$

where the lift curve slope is assumed to be linear and C is the Prandtl correction factor for the fact that the number of blades is finite. This correction factor is given by [1],

$$C = \frac{2}{\pi} \cos^{-1} e^{-f}, \quad (2)$$

where,

$$f = \frac{N_b (R_p - r) \sqrt{1 + \lambda^2}}{2R_p \lambda}.$$

From Equation 1 and 2 the propeller and slipstream properties are calculated. In particular $a, a', \alpha, c_x, c_y, dT$ and dQ . The factors a and a' give the axial and circumferential induced velocities behind the propeller and determine the

propeller slipstream effects on the other aircraft components.

3 Nacelle model

A preliminary study revealed that the forces and moments on the nacelle are dominated by the Magnus effect. To estimate the influence of the Magnus effect the propeller slipstream rotational velocities about the nacelle are substituted by a vortex of equivalent strength,

$$\Gamma_{eq} = 2\pi v_t R_n, \quad (3)$$

where v_t is the rotational velocity of the propeller slipstream at the nacelle surface. This vortex is located on the centerline of the nacelle and induces the same rotational velocity as the propeller slipstream at the nacelle surface. The nacelle experiences a flow perpendicular to the centerline, because the nacelle has an inclination with respect to the free stream and is located in the upwash due to wing lift. The side force experienced by the nacelle is given by

$$F_y = k \int \rho v_z \Gamma_{eq} dx, \quad (4)$$

where k is a parameter which is 1 for a counter-clockwise propeller and -1 for a clockwise propeller seen from behind and v_z is the upwash perpendicular to the nacelle centerline.

4 Wing model

The wing model is based on the Prandtl lifting line theory. The horseshoe vortices are located at one quarter of the wing chord and the collocation points at three quarters of the wing chord. The strength of each vortex is calculated by the method described in Katz and Plotkin [3]. The induced velocity of each vortex perpendicular to the wing plane can be written as an influence matrix \hat{A} times the vortex strength $\vec{\Gamma}$. With the boundary condition of zero velocity perpendicular to the wing plane the vortex strength becomes,

$$\vec{\Gamma} = \hat{A}^{-1} \vec{V}_\infty \cdot \vec{n}. \quad (5)$$

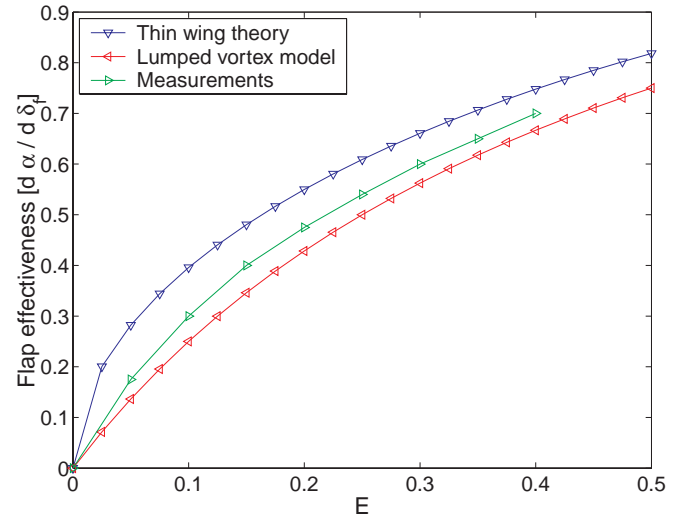


Fig. 1 Flap effectiveness.

This equation is the basis of the wing model and is extended to include flap settings and account for the fuselage and nacelles. These extensions are discussed in the following paragraphs.

Including the effect of the flaps The flap is modelled by a vortex on the quarter chord of the flap. The increase in lift of the airfoil with flaps deployed is given by the flap effectiveness. For the current model this is given by,

$$\frac{d\alpha}{d\delta} = \frac{3E}{2E + 1}, \quad (6)$$

where,

$$E = \frac{c_f}{c_f + c_w}. \quad (7)$$

Plotting the flap effectiveness by the lumped vortex model, the thin wing theory and measurement data gives the results presented in Figure 1. The flap effectiveness is underestimated by the current model. The approximation is better than by thin wing theory. Furthermore, because the lumped vortex model is easily implemented in the Prandtl lifting line theory it is preferred over the thin wing theory.

Including the effect of the fuselage The presence of the fuselage disturbs the flow about the wing in two ways

- A fuselage at an angle of attack locally increases the free stream velocities.
- The wing lift changes the flow about the fuselage which causes the lift-carry-over effect. This in turn changes the flow and the lift on the wing.

The first effect is included by increasing the free stream velocities according to the transformation method of Multhopp ([7],[10]). The coordinate transformation is given by

$$\Re\left(\frac{d\bar{u}}{du}\right) = \Re\left(1 - \frac{R_F^2}{u^2}\right). \quad (8)$$

The second effect is included by mirroring the wing vortices in the fuselage according to the method of Lennertz [1]. The location of the mirror vortices is given by,

$$\begin{bmatrix} y \\ z \end{bmatrix}_M = \frac{R_F^2}{y^2 + z^2} \begin{bmatrix} y \\ z \end{bmatrix}. \quad (9)$$

This method does not account for the bound vortices on the wing. Giesing [2] accounts for these by placing an doublet distribution over the centerline of the fuselage. These effects are assumed to be small because the doublet strengths found are negligible. Therefore this has not been implemented.

Including the effect of the nacelles To estimate the effect of the nacelles the wing vortices are mirrored in the nacelle. From these preliminary calculations the effect of the nacelles on the lift distribution was found to be significant whereas the effect on the yawing moment was negligible.

5 Validation of the propeller–nacelle–wing model by measurements

The calculation results for the configuration with propeller, nacelle and wing are compared to the measurements performed by Mannée [6]. The wind-tunnel model is described in Appendix A. The propeller on the working engine can rotate only clockwise the other propeller is substituted

by a spinner. The measurements are therefore performed by positioning the live engine on either the port side, for outboard up rotation (OU), or starboard side, for inboard up rotation (IU). In this paper the interest lies in the additional moment due to propeller slipstream interference and therefore the measurements on the starboard side have been switched sign as if the rotation direction of the port engine had been changed only. This allows for a direct comparison of interference effects in one plot with all moments having the same sign. A positive yawing moment is chosen in the direction of the static propeller moment, which is the thrust times the moment arm. The thrust coefficient is defined as the model drag with engine-off minus the model drag with engine-on, made dimensionless by the dynamic pressure and the propeller disc area,

$$T_c = \frac{D_{T=0} - D_{T \neq 0}}{\frac{1}{2}\rho V_\infty^2 S_p} = \frac{T - D_i}{\frac{1}{2}\rho V_\infty^2 S_p}, \quad (10)$$

where D_i is the propeller interference drag on the configuration.

The results for the configuration without flaps are given in Figure 2. The correlation between measurement and calculation data is good. Adding flaps to the configuration gives the results as shown in Figure 3. This correlation is still good, however the critical engine with the largest yawing moment, inboard up, shows an underestimation. The computed yawing moment coefficient has even decreased with respect to the static moment coefficient, in contrast with experimental data.

6 Flow field behind the wing

The flow field behind the wing mainly determines the force and moment due to the vertical tail. This flow field consists of the wing trailing vortex sheet and the propeller slipstream. Both the model of the wing trailing vortex sheet and the propeller slipstream are based on the time stepping method,

$$\begin{bmatrix} x \\ y \\ z \end{bmatrix}_N = \begin{bmatrix} x + dx \\ y + \frac{v_y}{v_x} dx \\ z + \frac{v_z}{v_x} dx \end{bmatrix}, \quad (11)$$

where the velocities are determined by four components

- Free stream
- Vortex field
- Fuselage
- Propeller slipstream

For the propeller slipstream the situation is more complicated because the position, shape and vortex strength of the slipstream vary. The induced velocities are discussed in the following paragraphs.

Wing trailing vortex sheet The effect of the vortex field on itself is determined by assuming semi-infinite straight vortices. One endpoint of these vortices is located at one quarter of the wing chord. The induced velocity due to one vortex at a distance (y, z) from the vortex core is given by,

$$\begin{bmatrix} dv_y \\ dv_z \end{bmatrix} = \frac{d\Gamma(\cos\phi + 1)}{4\pi(y^2 + z^2)} \begin{bmatrix} -z \\ y \end{bmatrix}, \quad (12)$$

where ϕ is the angle between the vortex centerline and the line through the point of interest (y, z) and the finite end point of the vortex (at one quarter chord). The total velocity increase is then given by integrating over all vortices.

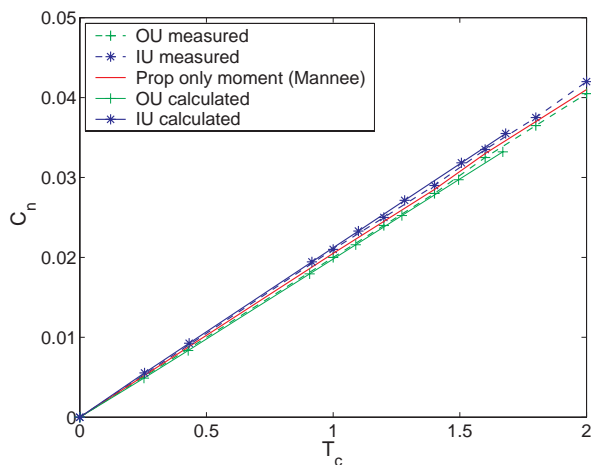


Fig. 2 Yawing moment coefficient for the propeller, nacelle and wing configuration, without flaps.

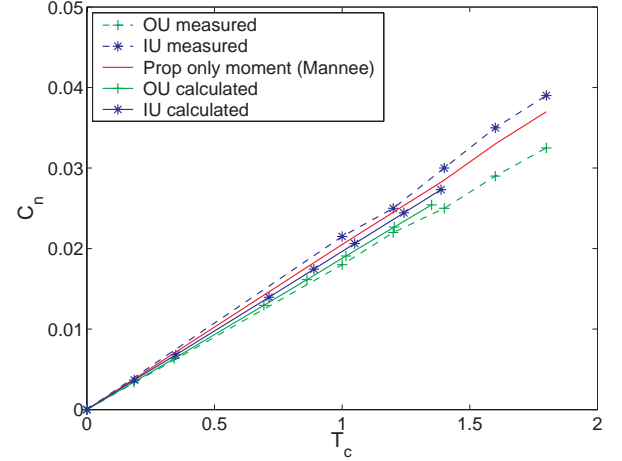


Fig. 3 Yawing moment coefficient for the propeller, nacelle and wing configuration, with flaps.

Fuselage The effect of the fuselage is three-fold. First the local increase of free stream velocity due to the blockage of the fuselage. Second the lift-carry-over effect modelled by the mirror vortices. And third the influence of the decreasing fuselage radius. The first two effects are discussed in Section 4.

The decrease of the fuselage radius is included by assuming a source distribution at the fuselage centerline. The velocity due to this source distribution needs to be tangential to the fuselage surface as there can be no flow through the surface. With the known shape of the fuselage the source strength can be determined. The displacement of a vortex at (y, z) due to the decreasing radius becomes

$$\begin{bmatrix} dy \\ dz \end{bmatrix} = \frac{dR_F}{dx} \frac{R_F}{y^2 + z^2} \begin{bmatrix} y \\ z \end{bmatrix} \quad (13)$$

Propeller slipstream The velocities induced by the propeller slipstream are calculated by introducing a propeller slipstream element. The assumptions made to form this element are derived from the surface vorticity panel method by Da-Qing Li [4]. For design purposes a time averaged propeller slipstream is used. This is equivalent to a propeller with an infinite number of blades. The plane of interest is the vertical tail plane. In this location the slipstream is fully converged and all vorticity is concentrated in a core vortex and a

slipstream surface [12]. The slipstream surface is divided in a number of panels on which the vorticity is constant. To reduce the calculation time a slipstream element is created based on the assumption that the influence of the propeller slipstream is dominated by the panels close to the point of interest. This element has a variable slipstream shape and vorticity strength and can move with the free stream vector. A schematic is given in Figure 4.

The velocity induced by a single panel is given by

$$\vec{v} = \frac{\vec{\gamma}}{4\pi} \times \iint_S \nabla \left(-\frac{1}{r} \right) dS \quad (14)$$

and the vorticity strength for a panel i, j in axial direction

$$\begin{aligned} \gamma_{\xi_{i+1,j}} = & \frac{l_1}{l_3} \gamma_{\xi_{i,j}} - \frac{w_{i,j}}{2l_3} (\gamma_{\xi_{i,j-1}} - \gamma_{\xi_{i,j+1}}) + \\ & \frac{w_{i,j}}{2l_3} \left[S_{14} (\gamma_{\xi_{i,j}} + \gamma_{\xi_{i,j-1}}) - \right. \\ & \left. S_{23} (\gamma_{\xi_{i,j}} + \gamma_{\xi_{i,j+1}}) \right], \end{aligned} \quad (15)$$

and in circumferential direction

$$\frac{\Delta(p_t)_\eta}{\rho} = -\gamma_\xi V_{\zeta_m} + \gamma_\zeta V_{\xi_m}. \quad (16)$$

For angles of attack close to zero this method works very well. For larger angles of attack the vorticity tends to go to infinity. From the measurements performed by Mannée it is found that the propeller slipstream does not touch the aircraft directly. The precise shape and strength of the propeller slipstream is therefore of secondary importance. The slipstream surface is therefore chosen to be circular and of constant strength [11].

7 Empennage

The empennage is modelled in the same way as the wing. This includes the blockage due to the fuselage and lift-carry-over effects. The differences lie in the fact that the velocity at the vertical tail is also affected by the presence of the wing trailing vortex field and the influence of the horizontal and vertical tail on each other.

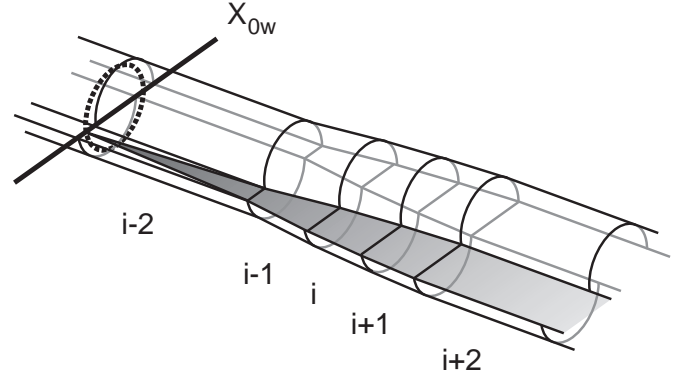


Fig. 4 Slipstream tube element

Comparing the calculated and measured yawing moment coefficients for the wind-tunnel model of Mannée shows a good correlation for the configuration without flaps, Figure 5. The configuration with flaps deployed shows a 30% underestimation. The vertical tail loading is determined by the cross flow at the tail. Assuming that the tail is modelled correctly by the horseshoe vortices, the error must lie in the wing trailing vortex field and propeller slipstream induced velocities.

8 Fuselage

The effect of the fuselage on the wing is already discussed in section 4. This included the additional upwash due to the blockage of the fuselage

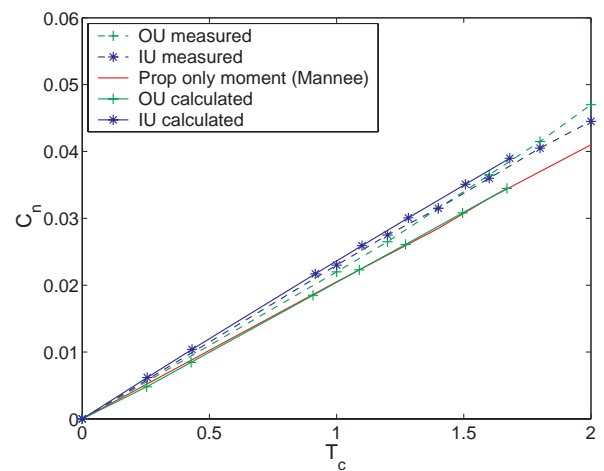


Fig. 5 Yawing moment coefficient for the propeller, nacelle, wing and tail configuration, without flaps.

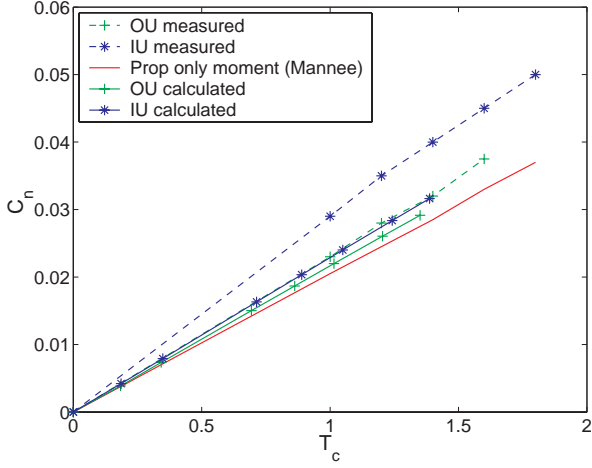


Fig. 6 Yawing moment coefficient for the propeller, nacelle, wing and tail configuration, with flaps.

and the lift-carry-over effect on the fuselage due to the presence of a lifting wing. The effect of the fuselage on the wing trailing vortex sheet is discussed in section 6. The effect of the fuselage on the presence of the empennage is discussed in section 7.

Part of the moment due to the fuselage is caused by the fuselage in a cross flow as was described by Munk [8]. Due to the presence of the propeller and an asymmetrical lift distribution the pressure on the fuselage is no longer axis-symmetrical, which results in a force and moment.

The moment due the cross-flow or angle of attack is given by,

$$M_F = \rho V^2 \alpha_F \int_0^{l_F} \pi R_F^2 dx \quad (17)$$

In the current situation the angle α_F and velocity V are not constant with axial position x . The moment equation is therefore rewritten as,

$$M_F = \rho \pi \int_0^{l_F} V^2 \alpha_F R_F^2 dx \quad (18)$$

A similar equation can be derived for the yawing moment

$$N_F = -\rho \pi \int_0^{l_F} V^2 \beta_F R_F^2 dx \quad (19)$$

Note the minus sign, caused by the positive sideslip angle which results in a negative yawing

moment.

The second contribution is the difference in pressure on the port and starboard side. This difference is caused by the difference in induced velocities in the wing trailing vortex field. The pressures due to these induced velocities are calculated on four points on the fuselage by Bernouilli,

$$p_n = p_t - \frac{1}{2} \rho (V_\infty + v_n)^2. \quad (20)$$

For the yawing moment the difference in pressure on the port and starboard side is used. Per definition the pressure difference is zero at the top and bottom of the fuselage. The pressure distribution is assumed to be triangular per section and the force per fuselage length becomes

$$\frac{dF}{dx} = \Delta p_{12} R_F, \quad (21)$$

where,

$$\Delta p_{12} = \frac{1}{2} \rho V_\infty^2 (2 + v_1 + v_2) (v_2 - v_1).$$

Increasing the number of points from four to eight has no significant effect on the total moment.

Comparing the calculated and measured yawing moment coefficients for the configuration without vertical tail shows results that are similar. Both configurations, without flaps (Figure 7) and with flaps (Figure 8), show a slight overestimation of the yawing moment.

Including the vertical tail in the calculations shows results similar to the configuration without fuselage. The configuration without flaps (Figure 9) shows a good correlation with the measurements. The configuration with flaps deployed shows an underestimation of approximately 30% as can be seen in Figure 10. This is again contributed to a underestimated cross flow at the tail. It can be concluded that the wing trailing vortex sheet and propeller slipstream induced velocities are incorrectly calculated.

A comparison of the wing lift increment due to the propeller slipstream reveals that the calculated lift increment is smaller than the measured lift increment with flaps deployed. This is true

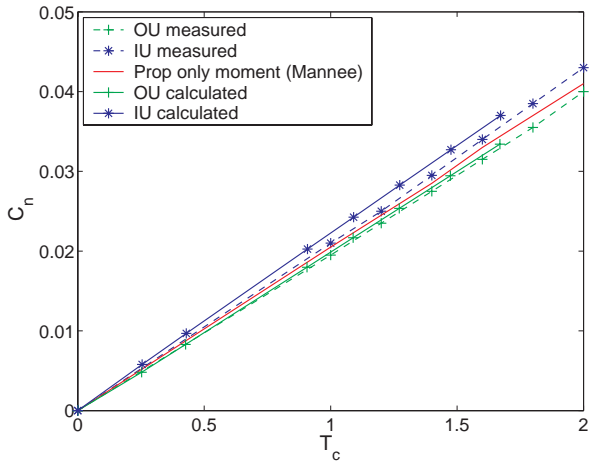


Fig. 7 Yawing moment coefficient for the propeller, nacelle, wing and fuselage configuration, without flaps.

for both the IU and OU rotating propeller. This is one cause for the incorrect wing trailing vortex field.

The second error can be found when investigating the wing trailing vortex sheet itself. Figure 11 shows the wing trailing vortex sheet for an IU rotating propeller. Striking is the irregular shape of the vortex sheet near the fuselage. The cross flow on the vertical tail is dominated by the influence of the vortices close to the tail. Due to this irregular vortex movement the validity of the vortex location is questionable. The irregular movement of the vortices near the fuselage is caused by the large gradient in vortex strength due to the presence of the inboard flap tip. The induced velocities are therefore very large. Increasing the number of steps in the vortex sheet does not have the desired effect of a smoother surface. This is therefore not seen as the solution because the calculation time increases drastically. The wing trailing vortex sheet model is not suited to model complex configurations with a wing, flap and fuselage.

9 Conclusions

The aircraft components are modelled by potential theory and compared to the measurements performed by Mannée.

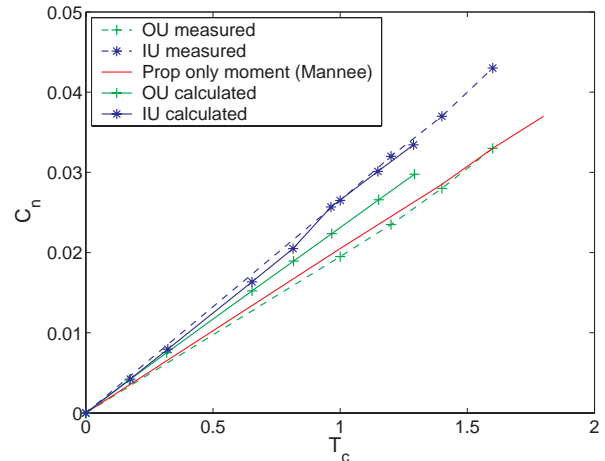


Fig. 8 Yawing moment coefficient for the propeller, nacelle, wing and fuselage configuration, with flaps.

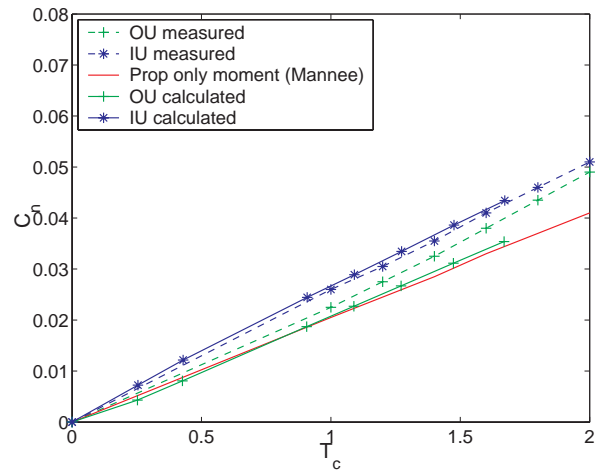


Fig. 9 Yawing moment coefficient for the propeller, nacelle, wing, fuselage and tail configuration, without flaps.

The calculation and measurement results for yawing moment coefficient of the configuration without flap deflection show good correlation. The correlation in yawing moment coefficient is underestimated by 30% with the flaps deployed especially for the configurations with vertical tailplane. This suggests that the cross flow at the tail is calculated incorrectly. Further investigation shows that the calculated wing lift distribution and therefore the shape and strength of the wing trailing vortex field were incorrectly modelled. In particular the lift distribution at the in-

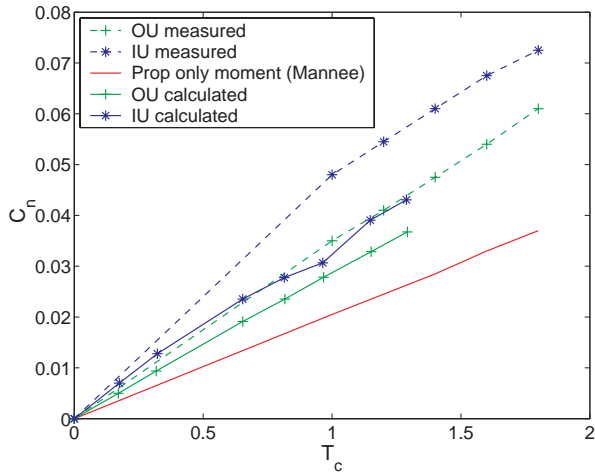


Fig. 10 Yawing moment coefficient for the propeller, nacelle, wing, fuselage and tail configuration, with flaps.

board tip of the flap and the resulting trailing vortices are highly sensitive to the numerical modelling of that region. The strength and position of these trailing vortices close to the vertical tail are the most probable cause for the errors in the yawing moment.

References

- [1] W.F. Durand, editor. *Aerodynamic theory*, volume IV. Springer, 1935.
- [2] J.P. Giesing. Lifting surface theory for wing-fuselage combination. Report DAC-67212, DAC, 1968.
- [3] J. Katz and A. Plotkin. *Low speed aerodynamics*. Cambridge university press, second edition, 2001.
- [4] Da-Qing Li. *Investigation on propeller-rudder interaction by numerical methods*. Phd thesis, Chalmers University of Technology, 1994.
- [5] J. Mannée. Windtunnel investigation of the influence of the aircraft configuration on the yawing- and rolling moments of a twin-engined propeller driven aircraft with one engine inoperative. Report NLL A-1508 B, NLL, 1962.
- [6] J. Mannée. Windtunnel onderzoek naar de invloed van de vliegtuigconfiguratie op gier- en rolmoment ten gevolge van het uitvallen van een motor bij een tweemotorig schroefvliegtuig. Report NLL A-1508 A, NLL, 1963.

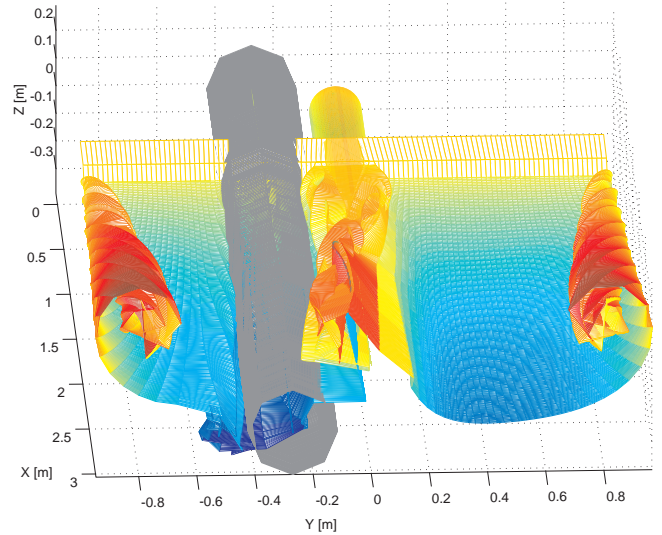


Fig. 11 Wing trailing vortex sheet for the configuration with inboard up rotating propeller, fuselage and flaps deployed.

- [7] H. Multhopp. Aerodynamics of the fuselage. Technical Memorandum 1036, National Advisory Committee for Aeronautics, 1942.
- [8] M.M. Munk. The aerodynamic forces on airship hulls. Report 184, National Advisory Committee for Aeronautics.
- [9] P. Rauhut. Modelling of the slipstream effects on the static lateral and directional stability and control of a single engine propeller aircraft. Master's thesis, Delft university of technology, 2002.
- [10] M. Renooij. Propeller slipstream effects and wing-fuselage lift carry-over effects on the stability of a single engine propeller airplane. Master's thesis, Delft university of technology, 2005.
- [11] M.J.T. Schroijen. Propeller installation effects on lateral stability and control of multi-engine propeller aircraft. Master's thesis, Delft University of Technology, to be issued June 2006.
- [12] L.L.M. Veldhuis. *Propeller wing aerodynamic interference*. Phd thesis, Delft University of Technology, 2005.

A Wind-tunnel model as used by Mannee

The wind-tunnel measurements as performed by Mannée in reference [6] and [5] are used for val-

idation, because of the multitude of configurations examined. The wind-tunnel measurements were performed at relatively low speeds ($39m/s$) and large angles of attack: 5° for the configuration without flaps and 5.8° for the configuration with 30° flap deflection. The configuration used for the measurements without fuselage is given in Figure 12. The configuration with fuselage is given in Figure 13 and Figure 14. In this last figure the moment point of the configuration is also given, 40% of the wing chord. In all configurations used for validation the nacelle is offset 275 millimeter from the fuselage centerline. The positive x -axis is pointing from the nose to the rear of the aircraft, the positive y -axis is pointing to the starboard side and to complete the right hand reference frame the z -axis is pointing upward. The yawing moment is chosen positive along the negative z -axis, to have a positive static propeller yawing moment for a live port engine.

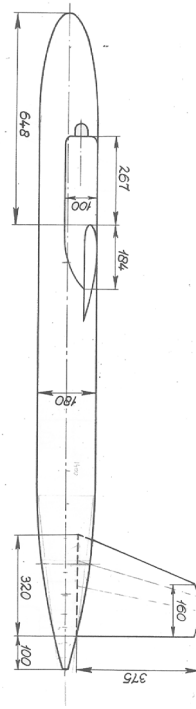


Fig. 13 Configuration with fuselage, side view, dimensions in millimeters.

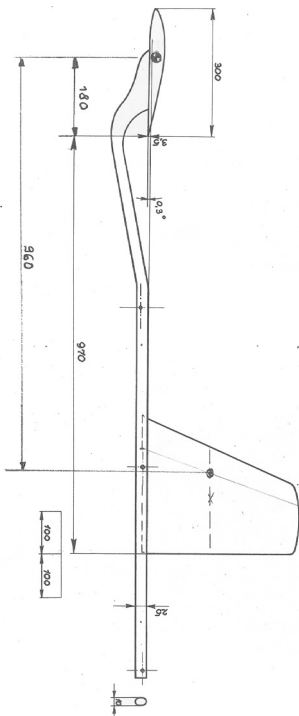


Fig. 12 Configuration without fuselage, dimensions in millimeters.

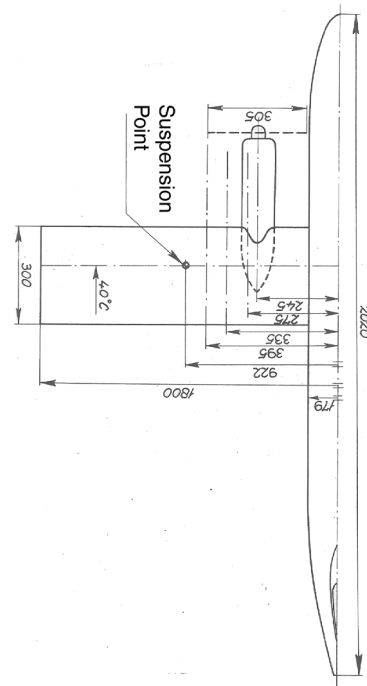


Fig. 14 Configuration with fuselage, top view, dimensions in millimeters.